RAA 2016 Vol. **16** No. **3**, 41 (8pp) doi: 10.1088/1674–4527/16/3/041
http://www.raa-journal.org *http://iopscience.iop.org/raa*

***R**esearch in*
***A**stronomy and*
***A**strophysics*

Kinematic properties of the dual AGN system J0038+4128 based on long-slit spectroscopy

Yang-Wei Zhang[1,5], Yang Huang[3], Jin-Ming Bai[1,2], Xiao-Wei Liu[3,4] and Jian-Guo Wang[1,2]

[1] Yunnan Observatories, Chinese Academy of Sciences, Kunming 650011, China; *zhangyangwei@ynao.ac.cn*
[2] Key Laboratory for the Structure and Evolution of Celestial Objects, Chinese Academy of Sciences, Kunming 650011, China; *baijinming@ynao.ac.cn*
[3] Department of Astronomy, Peking University, Beijing 100871, China; *yanghuang@pku.edu.cn*
[4] Kavli Institute for Astronomy and Astrophysics, Peking University, Beijing 100871, China
[5] University of Chinese Academy of Sciences, Beijing 100049, China

Received 2015 April 24; accepted 2015 September 24

Abstract The study of kiloparsec-scale dual active galactic nuclei (AGN) provides important clues for understanding the co-evolution between host galaxies and their central supermassive black holes undergoing a merging process. We present long-slit spectroscopy of J0038+4128, a kiloparsec-scale dual AGN candidate, discovered recently by Huang et al., using the Yunnan Faint Object Spectrograph and Camera (YFOSC) mounted on the Lijiang 2.4-m telescope administered by Yunnan Observatories. From the long-slit spectra, we find that the average relative line-of-sight (LOS) velocity between the two nuclei (J0038+4128N and J0038+4128S) is about 150 km s^{-1}. The LOS velocities of the emission lines from the gas ionized by the nuclei activities and of the absorption lines from stars governed by the host galaxies for different regions of J0038+4128 exhibit the same trend. The same trend in velocities indicates that the gaseous disks are co-rotating with the stellar disks in this ongoing merging system. We also find several knots/giant H II regions scattered around the two nuclei with strong star formation revealed by the observed line ratios from the spectra. Those regions are also clearly detected in images from *HST* $F336W/U$-band and *HST* $F555W/V$-band.

Key words: techniques: spectroscopic — galaxies: kinematics and dynamics — galaxies: active — galaxies: interactions — galaxies: nuclei — galaxies: individual (J0038+4128)

1 INTRODUCTION

Almost all massive galaxies are believed to host central supermassive black holes (SMBHs) (Richstone et al. 1998). During the merger of gas-rich galaxies, active galactic nuclei (AGN) will be triggered because a large amount of gas can be sent to the central SMBHs by tidal interactions (Hernquist 1989; Kauffmann & Haehnelt 2000; Hopkins et al. 2008). The dual AGN are therefore natural products of two merging SMBHs triggered simultaneously by accreting gas in a gas-rich major merger (Begelman et al. 1980; Milosavljević & Merritt 2001). The search for dual AGN, especially for the ones on a kiloparsec-scale, is of extreme importance for understanding the relation between galaxy evolution and nuclei activities (Yu et al. 2011). However, at present, no more than a few dozen dual AGN have been found with separation between 1 and 10 kpc (e.g. Junkkarinen et al. 2001; Komossa et al. 2003; Ballo et al. 2004; Bianchi et al. 2008; Comerford et al. 2009a,b, 2011; Liu et al. 2010, 2013; Fu et al. 2011a; Koss et al. 2011; Rosario et al. 2011; McGurk et al. 2011, 2012, 2014; Barrows et al. 2012; Huang et al. 2014, hereafter H14). Moreover, current studies have a limited ability to identify kiloparsec-scale dual AGN rather than investigate the co-evolution between host galaxies and the central AGN.

Ionized gas and stellar kinematics of galaxies have been used to check whether merger processes are important in galaxy formation and evolution. Very recently, Villforth & Hamann (2015) investigated the ionized gas and stellar kinematics of four double-peaked [O III]λ5007 AGN. They found that the ionized gas generally follows the stars except for one showing an opposite trend between gas and stars. The only system with misaligned kinematics of gas and stars had a confirmed kiloparsec-scale dual AGN system using $Chandra$ X-ray data (Comerford et al. 2011). This system also shows no obvious tidal feature that may indicate the timescale of its coalescence of binary black holes is longer than $\sim$1 Gyr and the host galaxies are well relaxed. The other three systems with the same velocity trend between ionized gas and stars all show significant tidal features and are identified as dual AGN using optical or infrared data (McGurk et al. 2011; Fu et al. 2011a, 2012). It is still difficult to conclude that the aligned/misaligned kinematics of gas and stars is a gen-

eral behavior of early/late stages of dual AGN or just accidental. Hence, more long-slit observations of confirmed dual AGN will be very helpful to test this scenario.

Here, we present detailed kinematic analysis based on long-slit spectroscopy of J0038+4128, which is a kiloparsec-scale dual AGN candidate discovered recently by H14. J0038+4128 ($z = 0.0725$) was confirmed as a Seyfert 1–Seyfert 2 dual AGN system with two clear optical nuclei from the *Hubble Space Telescope* (*HST*) Wide Field and Planetary Camera 2 (WFPC2) images (see Fig. 1) with a small projected separation of 4.7 kpc. The southern component (J0038+4128S) is confirmed as a Seyfert 1 galaxy with a broad Lyα emission line (H14). The northern component (J0038+4128N) is confirmed as a Seyfert 2 galaxy with narrow lines (H14). This system is undergoing strong interactions and shows two pairs of bi-symmetric arms which are observed in dual AGN for the first time. J0038+4128 is very bright and thus allows us to obtain high quality spectra to study the kinematics of both ionized gas and stars, which also can enable us to investigate the relations among star formation, nuclear activity and galaxy evolution (Keel 1996; Colpi & Dotti 2011; Yu et al. 2011; Shields et al. 2012; Kormendy & Ho 2013).

The paper is organized as follows: The observations and data reductions are described in Section 2. The results, as well as discussions, are presented in Section 3. Finally, we summarize our main conclusions in Section 4. We adopt a ΛCDM cosmology with $\Omega_{\rm m}$ = 0.3, Ω_{Λ} = 0.7 and H_0 = 70 km s^{-1}Mpc^{-1} throughout the article. All quoted wavelengths are in units that are measured in air.

2 OBSERVATIONS AND DATA REDUCTIONS

Data were taken on the night of 2013 November 10 with the 2.4-m telescope at Lijiang Observatory (hereafter LJT; Zhang et al. 2012). The weather on that night was clear and had excellent seeing ($\sim 1.0''$). To fully subtract the cosmic rays and achieve high spectral signal-to-noise SNR ratio, three exposures were taken with the Yunnan Faint Object Spectrograph and Camera (YFOSC; Zhang et al. 2012) G8 grating through a slit width of $1.0''$ ($R \sim 2200$, $\lambda = 5100 - 9600$Å) for a total integration time of 6900 s (2100 s, 2100 s and 2700 s for each exposure). The pixel size of the YFOSC CCD chip is $0.283''$ per pixel. As shown in Figure 1, the slit is positioned to view both the centers of the two nuclei, J0038+4128N and J0038+4128S, simultaneously.

All the data reduction was performed with IRAF and IDL. The data were bias subtracted, flat-field calibrated, cosmic rays were removed, and wavelength calibration and flux calibration were performed with ESO spectral flux standard star (BD+25 4655), which was also observed on that night. The wavelength and flux calibrations were all performed in 2D. The distortions of the wavelength solution in the spatial direction were also corrected with arc lines. The final accuracies of the 2D wavelength calibrations are better than 5–10 km s^{-1} as checked by sky emission lines. In order to better study the kinematics of J0038+4128, we extract 1D spectra of nine slices in the spatial direction from the final 2D spectrum. As shown in Figures 1 and 2, those slices represent different interesting regions (e.g. two nuclei and knots) of J0038+4128. Here, we note that each slice contains spectra from at least 5 pixels and no point spread function (PSF) corrections are applied to the 1D spectra, which were taken under conditions of good seeing ($\sim 1.0''$).

3 RESULTS AND DISCUSSION

3.1 Kinematics

As shown in Figure 2, the 2D long-slit spectrum clearly exhibits two sets of spectra that correspond to different rotation systems, which has already been discussed by H14 in detail. In the following subsections, we will focus on the kinematic properties of this system. In principle, the [O III]λ5007 and Hβ emission lines are very important to study the kinematics of this system and are also included in our observed spectrum. However, the instrumental efficiency in the bluest range (5100 - 5400 Å) of G8 is too low to obtain a good enough spectrum. Therefore, the lines (e.g. [O III]λ5007 and Hβ) in the bluest range are excluded in the following kinematic study.

To study the kinematics of J0038+4128, we use the lines available from the obtained 1D spectra of each slice mentioned before, including emission lines of Hα, [N II]$\lambda\lambda 6549, 6583$, [S II]$\lambda\lambda 6717, 6731$ and absorption lines of MgIb$\lambda\lambda 5167, 5172$ and NaI$\lambda\lambda 5889, 5895$. The emission lines represent the properties of gas ionized by AGN activity in either the broad line region or the narrow line region and the absorption lines represent the properties of stars governed by the host galaxies. The spectra of those emission and absorption lines from different slices are presented in Figures 3 and 4, respectively. As Figure 3 shows, the quality of the emission lines is high enough for fitting. However, the fits for absorption lines are more difficult since the quality of the observed absorption lines is relatively poor considering their intrinsic weak strengths. Here, we only perform fits for absorption lines from slices with SNRs[1] better than 3σ. For some important regions (i.e. slices A/B and E/F) with absorption lines detectable smaller than 3σ, two slices are binned together to obtain good enough qualities ($\geq 3\sigma$). The SNRs of absorption lines from different slices are presented in Table 2. We fit those observed line profiles by single/multiple Gaussian(s) to obtain their central wavelengths and full width at half-maximums (FWHMs, without subtracting instrumental broadening). For Hα emission lines from slices B, C, D, E and F, both broad and narrow line regions are detectable. We then fit the observed line profiles by one Gaussian for [N II]λ6549, one Gaussian for [N II]λ6583, a pair of Gaussians for the Hα broad and narrow components with the same central wavelength and

[1] The SNRs of the absorption lines are defined as: the absolute peak value of the absorption lines over the standard deviation of the nearby continuum (1σ).

Table 1 Spatially Resolved Kinematics of Emission Lines for J0038+4128

Line	Slice	V (km s^{-1})	ΔV (km s^{-1})	FWHM (km s^{-1})	ΔFWHM (km s^{-1})
Hα	A	–124	3	226	11
Hα	B	–140	7	315	17
Hα	C	–42	11	486	28
Hα	D	26	17	486	44
Hα	E	53	10	479	27
Hα	F	9	12	444	28
Hα	G	189	4	325	13
Hα	H	88	5	317	12
Hα	I	135	3	273	10
H$\alpha^{\rm broad}$	B	–140	7	5841	413
H$\alpha^{\rm broad}$	C	–42	11	6059	218
H$\alpha^{\rm broad}$	D	26	17	5797	233
H$\alpha^{\rm broad}$	E	53	10	5719	198
H$\alpha^{\rm broad}$	F	9	12	5110	309
[NII] 6583	A	–109	9	359	41
[NII] 6583	B	–106	12	422	28
[NII] 6583	C	–66	10	602	26
[NII] 6583	D	–26	16	722	42
[NII] 6583	E	12	10	643	26
[NII] 6583	F	41	9	472	21
[NII] 6583	G	111	10	469	22
[NII] 6583	H	62	10	306	22
[NII] 6583	I	125	10	418	22
[SII] 6717	A	–82	13	310	30
[SII] 6717	B	–156	15	272	34
[SII] 6717	C	–12	12	434	27
[SII] 6717	D	11	17	480	41
[SII] 6717	E	52	13	440	30
[SII] 6717	F	85	22	434	52
[SII] 6717	G	123	13	349	30
[SII] 6717	H	65	14	281	32
[SII] 6717	I	107	10	181	23
[SII] 6731	A	–129	12	252	26
[SII] 6731	B	–273	28	493	70
[SII] 6731	C	–87	14	484	32
[SII] 6731	D	–15	18	431	43
[SII] 6731	E	5	15	463	37
[SII] 6731	F	32	25	450	60
[SII] 6731	G	76	23	399	55
[SII] 6731	H	42	23	337	53
[SII] 6731	I	113	18	289	41

Notes: V: The LOS velocities are given with respect to the average redshift (z = 0.0732). ΔV: The errors of LOS velocities. FWHM: Full width at half-maximum. ΔFWHM: The errors of FWHM.

Table 2 Spatially Resolved Kinematics of Absorption Lines for J0038+4128

Line	Slice	V (km s^{-1})	ΔV (km s^{-1})	SNR (σ)
MgIb 5167	A+B	–17	32	4.5
MgIb 5167	C	7	29	3.1
MgIb 5167	D	235	24	3.2
MgIb 5167	E+F	241	22	4.1
MgIb 5167	G	123	19	3.9
MgIb 5167	H	59	25	3.8
MgIb 5167	I	–	–	–
Na I 5889	A+B	–98	27	4.2
Na I 5889	C	–19	25	4.0
Na I 5889	D	8	22	4.3
Na I 5889	E+F	77	28	8.4
Na I 5889	G	52	26	8.2
Na I 5889	H	36	22	4.7
Na I 5889	I	–	–	–
Na I 5895	A+B	–67	28	4.2
Na I 5895	C	–45	24	4.0
Na I 5895	D	37	21	4.3
Na I 5895	E+F	52	23	8.4
Na I 5895	G	18	25	8.2
Na I 5895	H	–10	24	4.7
Na I 5895	I	–	–	–

Notes: V: The LOS velocities are given with respect to average redshift (z = 0.0732). ΔV: The errors of LOS velocities.

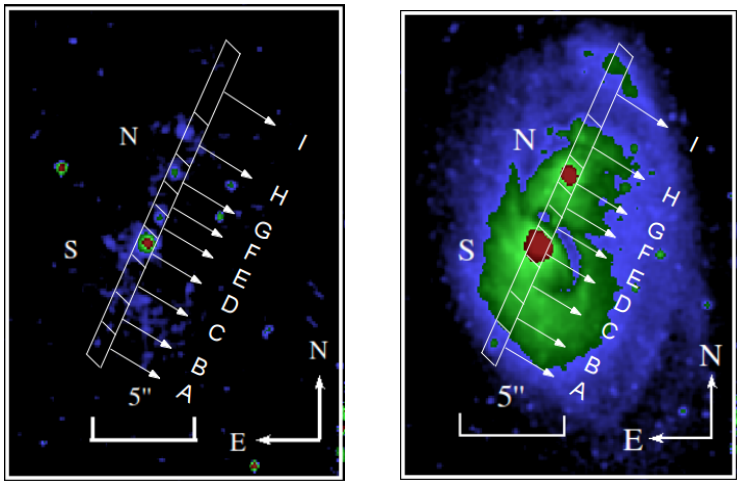

Fig. 1 These images of J0038+4128 are similar to figure 1 in H14. The image on the left was taken with *HST*/WFPC2 $F336W/U$-band and is shown in pseudocolor. The image on the right was acquired with *HST*/WFPC2 $F555W/V$-band and is also shown in pseudocolor. North is up and east is to the left. The spatial scale is also defined in each panel. The slit is positioned to view both nuclei simultaneously. The slit is further divided into nine slices, labeled with different letters, to extract 1D spectra of interesting regions.

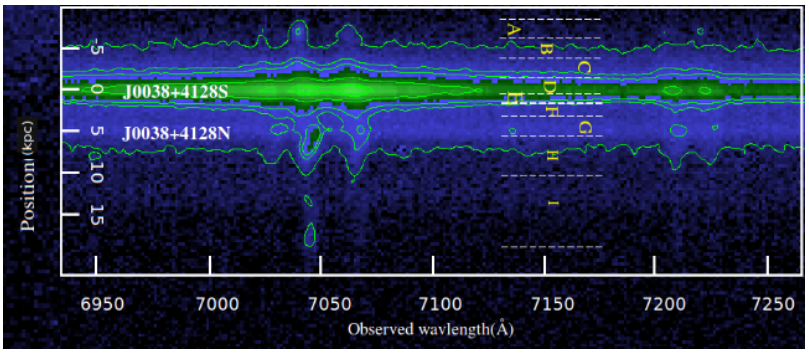

Fig. 2 Segment of the 2D long-slit spectrum of J0038+4128 that exhibits a spatially resolved broad Hα emission line and narrow emission lines (Hα+[N II]+[S II]) in the location of J0038+4128S and narrow emission lines (Hα+[N II]+[S II]) in the location of J0038+4128N. The locations of the different slices within the galaxy are labeled with letters and are shown in Fig. 1.

a linear polynomial for the continuum. The fits to other (emission and absorption) lines are similar to those of the Hα and [N II] lines. The results of all the fits for both emission and absorption lines are listed in Tables 1 and 2, respectively. The line-of-sight (LOS) velocities of different lines (four emission lines and three absorption lines) relative to an average redshift[2] of the J0038+4128, 0.0732, as a function of different regions (slices) are shown in Figure 5.

3.1.1 Relative LOS velocity

The relative LOS velocity is a very important parameter and has been incorporated into some dual AGN simulations (Wang & Yuan 2012; Blecha et al. 2013). J0038+4128S is represented by slices A, B, C, D, E and F and J0038+4128N is represented by slices F, G, H and I. The relative LOS velocity between J0038+4128S and J0038+4128N is about 150 km s^{-1}. The result is substantially smaller than the value derived by H14, which is 453 ± 87 km s^{-1}. The discrepancy is possible because the result of H14 is biased using two sets of spectra obtained by different instruments and wavelength ranges. The newly derived relative LOS velocity is still normal for a dual AGN system (generally 50-600 km s^{-1}; e.g. Comerford et al. 2012; Fu et al. 2011a,b, 2012; Barrows et al. 2013).

3.1.2 Kinematics of emission and absorption lines

Gaseous and stellar disks are largely co-rotating in normal galaxies, but counter-rotating cases of a gaseous disk with respect to a stellar disk are also seen in a few galaxies (Kuijken et al. 1996; Zeilinger et al. 2000; García-Burillo et al. 2003; Crocker et al. 2009; Nixon et al. 2012; Johnston et al. 2013; Ricci et al. 2014). The counter-rotating disks are possibly induced by a major merger (Corsini 2014). However, the detailed mechanism of this scenario is still

[2] The average redshift, 0.0732, is the mean measurement of the emission lines of Hα, [N II]λ6583 and [S II]$\lambda\lambda$6717, 6731. Derived from the average of two sets of spectra which were obtained by different instruments, the redshift ($z = 0.0725$) in H14 has a systematic error.

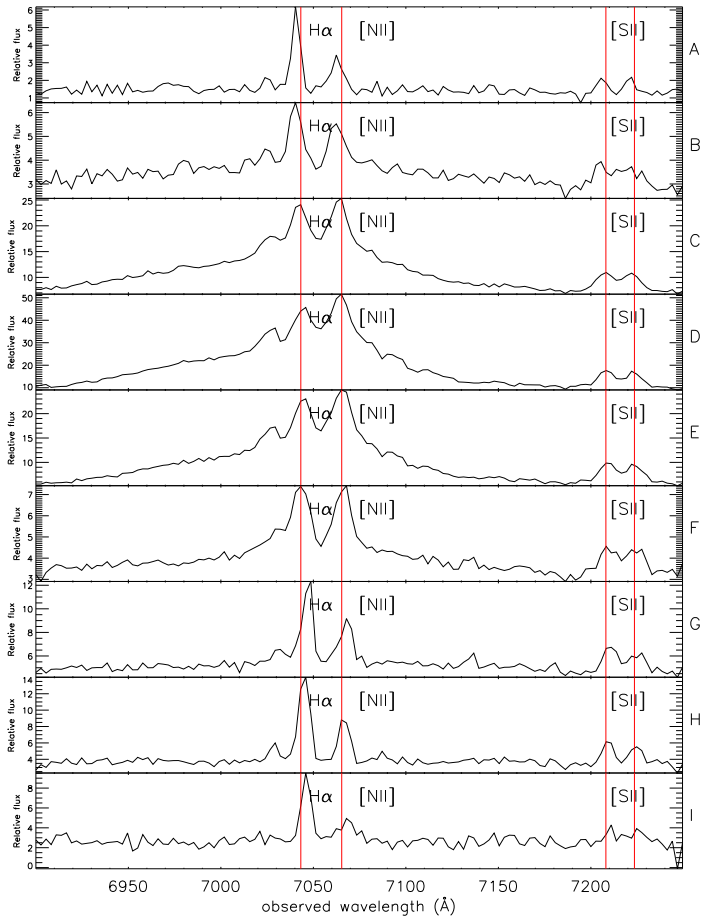

Fig. 3 1D spectra extracted along the nine slices for J0038+4128 showing Hα, [NII] and [SII] emission lines. Red lines indicate the detectable emission lines. Arbitrary flux units are shown for each panel to indicate relative line strengths.

Table 3 Properties of the Five Knots

Knots	ΔD_S (kpc)	ΔD_N (kpc)	Radii (kpc)	FWHM (km s^{-1})	log([NII]/Hα)	ΔV_k (km s^{-1})	Location
A_k	7.15	–	0.146	226	–0.21±0.02	149	south edge
B_k	5.96	–	0.117	315	–0.04±0.01	166	on arm
E_k	1.82	3.12	0.179	479	0.22±0.01	50	on arm
H_k	–	2.57	0.204	317	–0.28±0.03	101	on arm
I_k	–	7.65	0.496	273	–0.22±0.02	54	north edge

Notes: ΔD_S: Separation between knot and J0038+4128S. ΔD_N: Separation between knot and J0038+4128N. ΔV_k: Approximate velocity difference between knot and AGN.

unclear and needs more constraints from observations. Villforth & Hamann (2015) perform the first attempt to investigate the relationship between gaseous and stellar rotation disks in four double-peaked [O III]λ5007 AGN. The case of J0038+4128 studied here is essentially a dual AGN candidate, which can also provide important clues to test mechanisms associated with a (counter) rotating disk.

With the measured emission (representing gas) and absorption (representing stellar) lines in Tables 1 and 2 respectively, we compare the gaseous disk in J0038+4128S with stellar disks in J0038+4128S and compare the gaseous disk in J0038+4128N with stellar disks in J0038+4128N. The LOS velocities of emission lines and absorption lines display the same trend in both J0038+4128S and J0038+4128N, revealing that the gaseous and stellar disks are in a co-rotating system.

As Figure 1 shows, the tidal features indicate the dual AGN J0038+4128 are in an early merger stage. J0038+4128, in combination with the other three dual AGN (SDSS0952+2552, SDSS1151+4711, SDSS 1502+1115) found by Villforth & Hamann (2015), has a gaseous disk that co-rotates with respect to the stellar disk. Counter-rotation between gaseous and stellar disks is however only found in the dual AGN SDSS 1715+6008 (Villforth & Hamann 2015) which is in a late merger stage. The current results may imply that co-rotation between

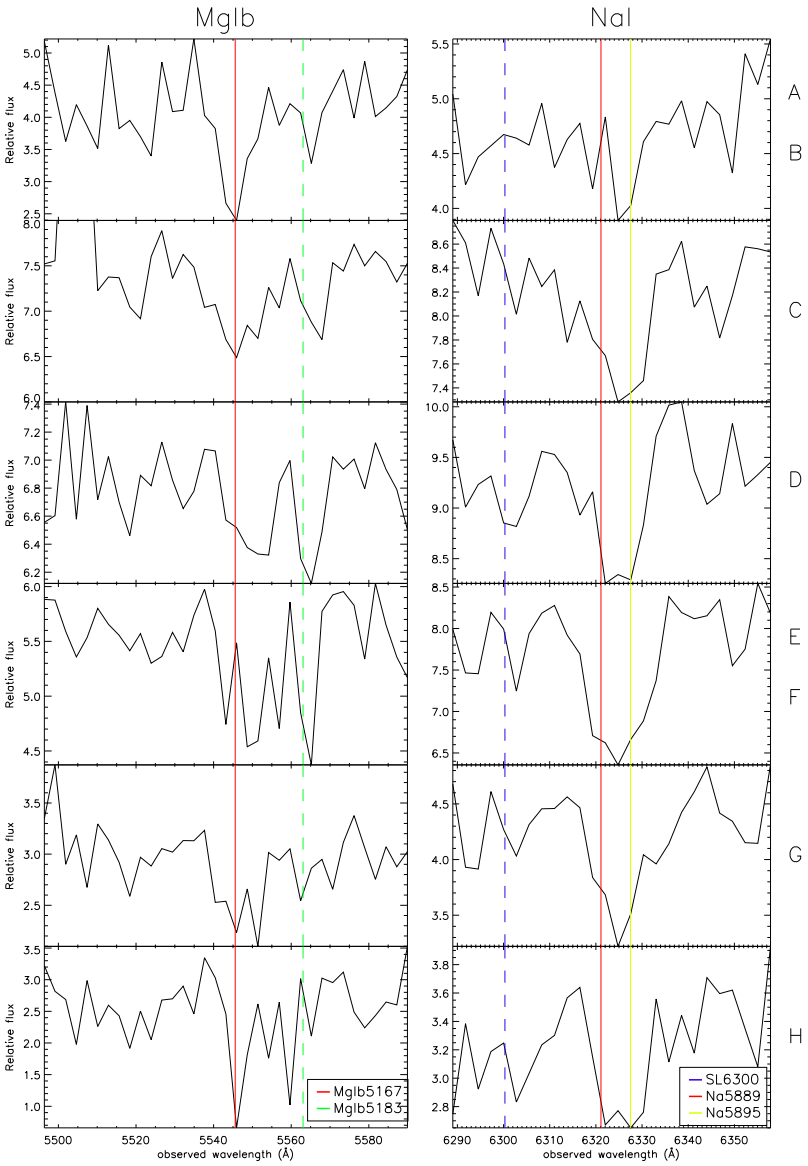

Fig. 4 1D spectra extracted along the nine slices for J0038+4128 showing MgIb$\lambda\lambda 5167, 5183$ and NaI$\lambda\lambda 5889, 5895$ absorption lines. Colored lines indicate the existing absorption lines. Arbitrary flux units are shown for each panel to indicate relative line strengths. SL6300 is the sky line in 6300 Å.

gaseous and stellar disks is normal behavior for dual AGN in the early merger stage and counter-rotation between gaseous and stellar disks may happen in the late merger stage of dual AGN. However, to better understand the relations between kinematics of gaseous and stellar disks in merger stages, a larger sample of dual AGN with 2D spectroscopy is needed.

3.1.3 Knots

As Figure 1 shows, there are more than a dozen compact knots scattered around the two nuclei of J0038+4128. We can infer that both nuclei in this dual AGN originally had gas rich predecessor galaxies which should be responsible for triggering this dual AGN and the surrounding knots. These knots are natural products of the galaxy merger (Villar-Martín et al. 2011) and their physical properties are very important for studying the merger galaxy. For the current spectroscopic observation, emissions from five knots are present in the long slit. We can extract 1D spectra of these knots within the slices labeled in Figure 1, which can provide us an opportunity to study the detailed properties of these five knots.

The spectra of five knots (A_k, B_k, E_k, H_k, I_k) are presented in Figure 3 and their associated properties are shown in Table 3. There are obvious discrepancies in values of FWHM between the knots on the arm and the knots on the edge, but other parameters show no discrepancies.

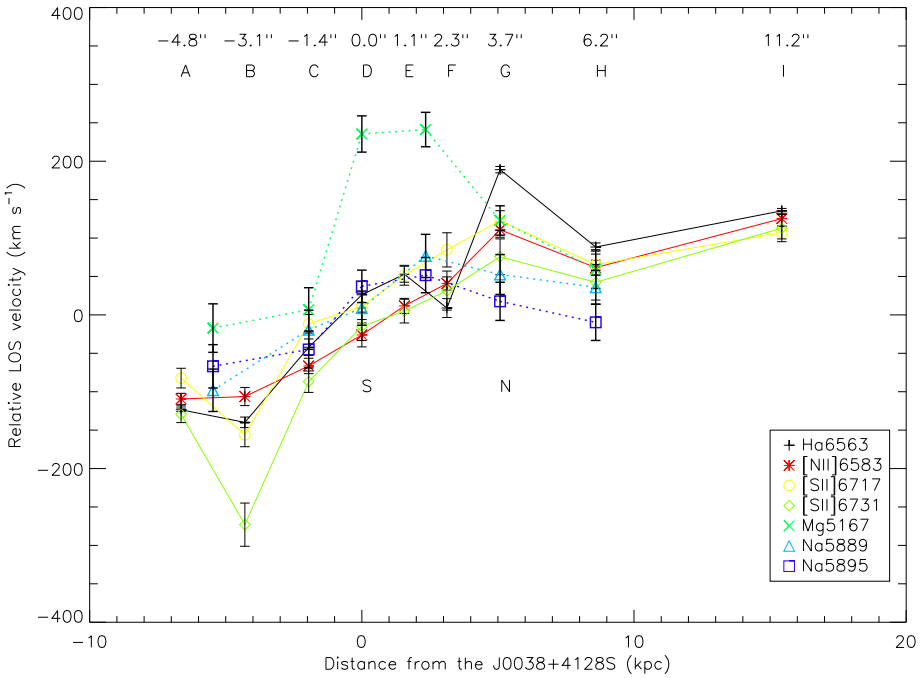

Fig. 5 Kinematic structure of different lines in J0038+4128. The location of different slices within the galaxy are labeled with letters and are shown in Figs. 1 and 2. N and S represent the cores of J0038+4128N and J0038+4128S respectively. The velocities are calculated by comparing the positions of emission lines with respect to the reference redshift. For details about the parameters used in the line fits, see in Tables 1 and 2.

As given in Table 3, the average FWHM of the Hα emission line corresponding to the three knots on the arm is 370 km s^{-1}, which is larger than 250 km s^{-1} corresponding to the two knots on the edge. The knots A_k and I_k on the edge are disconnected in the Figure 1 and the 2D spectra Figure 2, which lead us to infer that the knots A_k and I_k are being torn apart and thrown away from the center.

The knots show a wide range of sizes ranging from several pc to 400 pc (Miralles-Caballero et al. 2011). ULIRGs associated with spirals, interacting galaxies and mergers appear to aggregate in larger clumps with sizes in the range 0.1−1.5 kpc (Elmegreen et al. 2009; Förster Schreiber et al. 2011). Radii of the knots are approximately the half-light radius (Whitmore et al. 1993; Surace et al. 1998). These five knots have an average size of 0.228 kpc which is normal for dual AGN. The scattered compacted knots around this dual AGN system can be used to further investigate strong star formation activity. The merging system has extremely high star formation activity (Chapman et al. 2003; Frayer et al. 2003; Engel et al. 2010).

4 SUMMARY

We present a kinematic study of the dual AGN J0038+4128 based on long-slit spectroscopy obtained by LJT administered by Yunnan Observatories. From the long-slit spectroscopy, we find that the offset velocity between J0038+4128N and J0038+4128S is about 150 km s^{-1}. We also study the velocity trend between emission lines (ionized by gas) and absorption lines (governed by the host galaxy) and find they show the same trend. Combined with the long-slit spectroscopy study of the other four dual AGN candidates by Villforth & Hamann (2015), we find the co-rotation between gaseous and stellar disks is possibly at the early merger state and the counter-rotation is possibly at the late merger state. However, a larger sample of dual AGN with 2D spectroscopy is still needed to better understand the relations between kinematics of gaseous and stellar disks, and merger stages.

This dual AGN shows strong tidal morphologies, with more than a dozen compact knots scattered around the host galaxies. We have also studied the properties (e.g. FWHM, size) of five compact knots. The detailed properties of five knots are shown in Table 3. These scattered compact knots lead us to infer that this dual AGN is undergoing strong star formation activity.

We have started a systematic search for dual AGN and have found several dual AGN candidates since 2014 using the YFOSC on LJT of Yunnan Observatories. More dual AGN and their kinematic studies will be presented in future work.

Acknowledgements We acknowledge support by the staff of the Lijiang 2.4 m telescope. Funding for the telescope has been provided by CAS and the People's Government of Yunnan Province. We thank Fang Wang, Xu-Liang Fan, Cheng Cheng, Ju-Jia Zhang, Wei-Min Yi and Neng-Hui Liao for their help. The work of J. M. Bai is sup-

ported by the National Natural Science Foundation of China (Grant Nos. 11133006 and 11361140347) and the Strategic Priority Research Program "The Emergence of Cosmological Structures" of the Chinese Academy of Sciences (Grant No. XDB09000000). Y. Huang and X.-W. Liu acknowledge support by the National Key Basic Research Program of China (2014CB845700).

References

Ballo, L., Braito, V., Della Ceca, R., et al. 2004, ApJ, 600, 634
Barrows, R. S., Stern, D., Madsen, K., et al. 2012, ApJ, 744, 7
Barrows, R. S., Sandberg Lacy, C. H., Kennefick, J., et al. 2013, ApJ, 769, 95
Begelman, M. C., Blandford, R. D., & Rees, M. J. 1980, Nature, 287, 307
Bianchi, S., Chiaberge, M., Piconcelli, E., Guainazzi, M., & Matt, G. 2008, MNRAS, 386, 105
Blecha, L., Loeb, A., & Narayan, R. 2013, MNRAS, 429, 2594
Chapman, S. C., Windhorst, R., Odewahn, S., Yan, H., & Conselice, C. 2003, ApJ, 599, 92
Colpi, M., & Dotti, M. 2011, Advanced Science Letters, 4, 181
Comerford, J. M., Gerke, B. F., Newman, J. A., et al. 2009a, ApJ, 698, 956
Comerford, J. M., Griffith, R. L., Gerke, B. F., et al. 2009b, ApJ, 702, L82
Comerford, J. M., Pooley, D., Gerke, B. F., & Madejski, G. M. 2011, ApJ, 737, L19
Comerford, J. M., Gerke, B. F., Stern, D., et al. 2012, ApJ, 753, 42
Corsini, E. M. 2014, in Astronomical Society of the Pacific Conference Series, 486, Multi-Spin Galaxies, ASP Conference Series, ed. E. Iodice & E. M. Corsini, 51
Crocker, A. F., Jeong, H., Komugi, S., et al. 2009, MNRAS, 393, 1255
Elmegreen, D. M., Elmegreen, B. G., Marcus, M. T., et al. 2009, ApJ, 701, 306
Engel, H., Tacconi, L. J., Davies, R. I., et al. 2010, ApJ, 724, 233
Förster Schreiber, N. M., Shapley, A. E., Genzel, R., et al. 2011, ApJ, 739, 45
Frayer, D. T., Armus, L., Scoville, N. Z., et al. 2003, AJ, 126, 73
Fu, H., Zhang, Z.-Y., Assef, R. J., et al. 2011a, ApJ, 740, L44
Fu, H., Myers, A. D., Djorgovski, S. G., & Yan, L. 2011b, ApJ, 733, 103
Fu, H., Yan, L., Myers, A. D., et al. 2012, ApJ, 745, 67
García-Burillo, S., Combes, F., Hunt, L. K., et al. 2003, A&A, 407, 485
Hernquist, L. 1989, Nature, 340, 687
Hopkins, P. F., Hernquist, L., Cox, T. J., & Kereš, D. 2008, ApJS, 175, 356
Huang, Y., Liu, X.-W., Yuan, H.-B., et al. 2014, MNRAS, 439, 2927
Johnston, E. J., Merrifield, M. R., Aragón-Salamanca, A., & Cappellari, M. 2013, MNRAS, 428, 1296
Junkkarinen, V., Shields, G. A., Beaver, E. A., et al. 2001, ApJ, 549, L155
Kauffmann, G., & Haehnelt, M. 2000, MNRAS, 311, 576
Keel, W. C. 1996, ApJS, 106, 27
Komossa, S., Burwitz, V., Hasinger, G., et al. 2003, ApJ, 582, L15
Kormendy, J., & Ho, L. C. 2013, ARA&A, 51, 511
Koss, M., Mushotzky, R., Treister, E., et al. 2011, ApJ, 735, L42
Kuijken, K., Fisher, D., & Merrifield, M. R. 1996, MNRAS, 283, 543
Liu, X., Greene, J. E., Shen, Y., & Strauss, M. A. 2010, ApJ, 715, L30
Liu, X., Civano, F., Shen, Y., et al. 2013, ApJ, 762, 110
McGurk, R. C., Max, C. E., Rosario, D. J., et al. 2011, ApJ, 738, L2
McGurk, R. C., Max, C. E., Rosario, D. J., et al. 2012, in American Astronomical Society Meeting Abstracts, 219, #225.05
McGurk, R. C., Max, C. E., Medling, A., & Shields, G. A. 2014, in IAU Symposium, 304, ed. A. M. Mickaelian & D. B. Sanders, 371
Milosavljević, M., & Merritt, D. 2001, ApJ, 563, 34
Miralles-Caballero, D., Colina, L., Arribas, S., & Duc, P.-A. 2011, AJ, 142, 79
Nixon, C. J., King, A. R., & Price, D. J. 2012, MNRAS, 422, 2547
Ricci, T. V., Steiner, J. E., & Menezes, R. B. 2014, MNRAS, 440, 2419
Richstone, D., Ajhar, E. A., Bender, R., et al. 1998, Nature, 395, A14
Rosario, D. J., McGurk, R. C., Max, C. E., et al. 2011, ApJ, 739, 44
Shields, G. A., Rosario, D. J., Junkkarinen, V., et al. 2012, ApJ, 744, 151
Surace, J. A., Sanders, D. B., Vacca, W. D., Veilleux, S., & Mazzarella, J. M. 1998, ApJ, 492, 116
Villar-Martín, M., Humphrey, A., Delgado, R. G., Colina, L., & Arribas, S. 2011, MNRAS, 418, 2032
Villforth, C., & Hamann, F. 2015, AJ, 149, 92
Wang, X.-W., & Yuan, Y.-F. 2012, MNRAS, 427, L1
Whitmore, B. C., Schweizer, F., Leitherer, C., Borne, K., & Robert, C. 1993, AJ, 106, 1354
Yu, Q., Lu, Y., Mohayaee, R., & Colin, J. 2011, ApJ, 738, 92
Zeilinger, W. W., Vega Beltrán, J. C., Rozas, M., et al. 2000, in Astronomical Society of the Pacific Conference Series, 215, Cosmic Evolution and Galaxy Formation: Structure, Interactions, and Feedback, eds. J. Franco, L. Terlevich, O. López-Cruz, & I. Aretxaga, 214
Zhang J. J., Fan Y. F., Chang L., Wang C. J., & Yi W. M, 2012, Astronomical Research & Technology (Chinese), 9, 411